Hydrogeology Journal (2024) 32:983–998
https://doi.org/10.1007/s10040-024-02781-3

PAPER

The effect of fracture aperture and matrix permeability on suitability of the equivalent porous medium model for steady-state flow in fractured porous media

Di Han[1] · Lei Ma[1] · Jiazhong Qian[1] · Di Gao[2] · Haichun Ma[1] · Qiankun Luo[1] · Pengyu Qiu[1]

Received: 20 July 2023 / Accepted: 23 February 2024 / Published online: 8 March 2024

Abstract
The equivalent porous medium (EPM) method is an efficient approximate processing method for calculating groundwater yield taking into account the equivalent permeability coefficient of a fractured geological medium. The EPM method finds wide application in addressing various hydrogeological problems ranging from local to regional scales; however, the adequacy of the EPM model for evaluating water head and velocity distributions has not been comprehensively assessed. This study quantitatively investigated the influence of fracture and matrix permeability on the EPM model's suitability, defined by a 15% threshold for hydraulic-head prediction error, via numerical simulations. A fractured porous media system (fracture-matrix system) was considered as the prototype, and the EPM model simulation results were compared with those obtained using the discrete fracture-matrix (DFM) model. Results indicate a decrease in EPM suitability with larger fracture apertures. With a constant fracture aperture, the suitability of the EPM model increases as the matrix permeability increases. The size of the fracture aperture significantly affects the suitability of the EPM model, and it determines the point at which its suitability begins to increase and eventually stabilize. The fitted curve depicting the influence of matrix permeability on the suitability of the EPM model conforms to the Boltzmann formula, and the fracture aperture is linearly related to the parameter x_0 in the formula. The derived empirical formula enables quantitative assessment of the impact of fracture and matrix permeabilities on the suitability of the EPM model in fractured porous media.

Keywords Equivalent porous medium · Matrix permeability · Suitability · Fractured rocks · Statistical modeling

Introduction

Rock mass in the earth's crust is broken on scales from millimeters to kilometers, and fluid flow and mass transfer often occur in both the porous rock matrix and interconnected fracture networks for fractured porous rock. The matrix predominantly stores mass (e.g., hydrocarbons, water) and heat, governing long timescale processes. Fractures, in contrast to the rock matrix, exhibit significantly higher permeabilities and are widely recognized as the primary conduits for fluid and solute migration (Hu et al. 2022; Sweeney et al. 2020). Understanding the interaction between these physical systems is of utmost importance for numerous natural and engineering applications such as groundwater resource extraction (Luo et al. 2020), hydrocarbon extraction from unconventional reservoirs (Kim et al. 2021), CO_2 sequestration (Chen et al. 2022), geothermal energy extraction (Salimzadeh et al. 2019), and high-level radioactive nuclear waste disposal (Zhang et al. 2022).

Our ability to comprehend subsurface systems relies, in part, on the development of accurate numerical models capable of capturing the diverse mechanisms of physics occurring within fractures and the surrounding matrix, and their interactions. However, it is important to note that no single model currently exists as a universal solution. Models employed for simulating flow and transport processes in fractured porous media can be categorized into three types—equivalent porous medium (EPM) model, discrete fracture

✉ Lei Ma
Lei8505@hfut.edu.cn

✉ Jiazhong Qian
qianjiazhong@hfut.edu.cn

[1] School of Resources and Environmental Engineering, Hefei University of Technology, Hefei 230009, China

[2] Institute of Surface-Earth System Science, School of Earth System Science, Tianjin University, Tianjin 300072, China

network (DFN) model, and discrete fracture-matrix (DFM) model (Applegate and Appleyard 2022; Khafagy et al. 2022a, b; Wei et al. 2020). Each model utilizes a distinct set of underlying methods, which come with their own inherent advantages and disadvantages.

The accurate simulation of flow in fractured porous media hinges on effectively characterizing complex fracture network geometries and accurately representing the coupled flow dynamics within fractures and the surrounding matrix. The EPM, DFN, and DFM models address (or do not address) these issues in different ways. Specifically, the EPM model regards the fractured geologic medium as a continuum medium and considers that the permeability of the fractured geologic medium is equivalent to that of a continuum porous medium (Mortazavi et al. 2022; Wang et al. 2022a, b; Weijermars and Khanal 2019; Xue et al. 2022). The EPM model has been successfully applied to solve large-scale water yield problems in fractured geologic media, making it widely utilized in geological engineering practice (Chen et al. 2020; Scanlon et al. 2003; Song et al. 2018; Zhang et al. 2020). The EPM model provides a simplified approach for representing flow within fractured rock mass and is renowned for its ease of implementation compared to other models.

To more thoroughly consider the impact of fracture networks, some scholars have proposed multicontinuum methods building upon the foundation of the EPM model (Bosma et al. 2017; Sweeney et al. 2020). The dual-porosity model is a quintessential multicontinuum approach, which, to a certain extent, describes the phenomenon of preferential flow and accounts for the exchange of water flow between the fracture system and the matrix system. This method proves effective and suitable for reservoirs characterized by dense and extensive fracture distributions (Hu et al. 2021; Ma et al. 2023a, b; Pham and Falta 2022). However, its principal limitation lies in relying on empirical transfer functions for fluid transport between the matrix and fractures, leading to a homogenized fracture domain that substantially obscures detailed fracture information. In practice, the effectiveness of this method also requires assessment and validation.

The DFN model focuses solely on water flow within fractures and does not account for penetration into the rock matrix. It is a suitable method for accurately characterizing fracture geometry, spatial connectivity, and flow behavior (Feng et al. 2020; Huang et al. 2021; Khafagy et al. 2022a, b; Yaghoubi 2019). By excluding the matrix, the DFN model can utilize existing numerical methods that specifically address flow within fractures (Berrone et al. 2019; Geetha Manjari and Sivakumar Babu 2022); however, the DFN model necessitates a substantial amount of fracture investigation data and extensive computational effort, which limits its practical application in engineering. Furthermore, the absence of rock matrix representation restricts its applicability to specific scenarios, such as flow in impermeable rocks.

Unlike the DFN model, the DFM model explicitly represents both the fracture network and the surrounding porous matrix. Although the DFM model is newer compared to the DFN and EPM models, there are still implementation challenges that need to be addressed (Jia and Xian 2022; Mi et al. 2017; Zhao et al. 2019). The DFM model effectively captures the complexities of fracture network geometries and accurately represents the coupled flow dynamics within the fractures and the surrounding matrix, thus offering a high-fidelity representation of the fracture-matrix system. However, challenges related to meshing and numerical methods have restricted its applicability to simpler problems (Ţene et al. 2017; Wang et al. 2022a, b; Younes et al. 2023; Zhao et al. 2018). Generally, the DFM model represents the fracture network as (n—1)-dimensional fractures coupled with an (n)-dimensional mesh that represents the matrix. Consequently, the meshes utilized in the DFM model are inherently multidimensional, which introduces additional complexities in solving the governing equations for flow and transport (Hyman and Dentz 2021; Li et al. 2019, 2023; Liu et al. 2020).

Certain regional-scale and long-term hydrogeological problems necessitate more precise descriptions of water head or velocity distributions, particularly for applications such as hydrogeochemical evolution and nuclide migration within fractures. When using the DFN or DFM model, accurately characterizing all fractures becomes impractical due to limitations in current investigation techniques, high investigation effort, and associated costs. One possible approach to overcome these challenges is to utilize the EPM method, which reduces model complexity and computational cost by not explicitly including fractures in the models (Wei et al. 2021). To apply the EPM model, researchers introduced the concept of the representative elementary volume (REV) to describe the hydraulic characteristics of the equivalent continuum model in hydrogeology (Dou et al. 2019; Liang et al. 2019; Liu et al. 2021; Loyola et al. 2021). Researchers have proposed several methods to assess the occurrence of the REV through numerical simulations (Rong et al. 2013; Young et al. 2020); however, this evaluation method does not provide a clear criterion for assessing suitability.

Previous research indicates that the presence of fractures significantly influences the head value, and neglecting fractures can result in estimation errors in the groundwater quantity and velocity (Koohbor et al. 2020; Qi-Zhen et al. 2012; Xing et al. 2021a, b). Furthermore, various studies have demonstrated that fractures have a substantial impact on simulation results (Jarrahi et al. 2019; Zareidarmiyan et al. 2021; Zeng et al. 2021). However, a convenient and efficient method for evaluating the influence of fractures on the suitability of the EPM model is still lacking. The permeability of a fractured geologic medium is determined by many factors, among which the most important parameters are fracture permeability and matrix permeability (Baghbanan and Jing 2008; Bou Jaoude et al. 2022). Further, fracture permeability is mainly controlled by the fracture aperture. Some scholars have carried out a series of research projects on the seepage of fractured rock mass based on these factors (Bisdom et al. 2016; Dou et al. 2018; Mi et al. 2014); however, the influence of fracture aperture and matrix permeability of fractured rock mass on the suitability of the EPM model remains unclear.

The objective of this study, conducted within a two-dimensional (2D) framework, was to assess the impact of fracture aperture and rock matrix permeability on the suitability of the EPM model. To accomplish this, a 2D DFM prototype model was generated using statistical parameters of fractures from the Three Gorges Dam Project area in China. Subsequently, multiple sets of DFM models were created, varying the fracture aperture and matrix permeability of the fractured rock mass. The influence of these parameters on the suitability of the EPM model was analyzed. This study provides valuable insights into the impact of fracture aperture and matrix permeability on the suitability of the EPM method for fractured rock masses. The findings offer a scientific basis for determining the applicability of this method to address water-head-related hydrogeological issues in fractured geological media at specific sites.

Methodology

Two-dimensional (2D) discrete fracture-matrix model

The DFM model combines the advantages of the DFN model and the EPM model. The equations of water flow are established with the equivalent continuous medium model and discrete medium model, respectively, and then the coupling calculation is carried out according to the basic principle for establishing the DFM model, that is, the hydraulic heads at the contact of the two media are the same and the flow at the nodes is balanced. The finite element method can be used to solve the equation of the DFM model of seepage in fractured rock mass (Hu et al. 2022; Sweeney et al. 2020; Zheng et al. 2021)—for a more detailed introduction to the DFM model, refer to (Binda et al. 2021; Dodangeh et al. 2023; Ma et al. 2023a, b). This model can obviously consider the influence of fracture and matrix permeability on seepage at the same time.

Mathematical model of water flow in 2D discrete fractures

The DFN model considers that the rock mass itself is impermeable, and the fracture is regarded as a discrete independent model. The mathematical model representing the anisotropy of the medium is established with fracture parameters, to determine the real flow state of the fluid in the fracture network (Fu et al. 2013; Lopes et al. 2022; Su et al. 2022). The nomenclature is summarized in the Appendix.

In the fracture network, line elements and their two end nodes form the basic units. If node i is an endpoint of line element j, then element j is said to be connected to node i. The degree of node i is the number of line elements connected to it. Assuming the selection of a 2D fracture study domain ABCD, which includes fracture intersection point i, a closed curve passing through the midpoints of all connected line elements is constructed centered on point i, forming a representative domain. According to the assumption of single-phase incompressible fluid flow and the principle of mass conservation for steady seepage, the seepage equation within the representative domain can be written as:

$$\left(\sum_{j=1}^{N'} q_j\right)_i + Q_i = 0 \tag{1}$$

where q_j represents the flow rate into or out of node i through line element j; N' is the degree of node i; Q_i is the source-sink term at node i.

If there are N nodes and M line elements in the fracture study area, then N equations of the form of Eq. (1) can be formed, which can be written in matrix form as follows:

$$\mathbf{Aq} + \mathbf{Q} = 0 \tag{2}$$

where $\mathbf{A}$ is an aggregation matrix reflecting the aggregation relationship between the line elements and nodes in the fracture network. The matrix $\mathbf{A}$ has the number of rows equal to the number of nodes and the number of columns equal to the number of fracture line elements; $\mathbf{q} = \left(q_1, q_2, \cdots, q_N\right)^{\mathrm{T}}$; $\mathbf{Q} = \left(Q_1, Q_2, \cdots, Q_N\right)^{\mathrm{T}}$.

The specific discharge formula of incompressible fluid flow in a laminar regime within a fracture consisting of two parallel and smooth surfaces is given by the cubic law (He et al. 2021; Wang et al. 2020a, b; Xing et al. 2021a, b), as follows:

$$q = \frac{\gamma}{4\mu} J_{\mathrm{f}} \int_0^{b/2} \left(b^2 - 4y^2\right) dy = \frac{\gamma b^3}{12\mu} J_{\mathrm{f}} \tag{3}$$

The average velocity of water flowing through this fracture is:

$$V = \frac{\gamma b^2}{12\mu} J_{\mathrm{f}} = K_{\mathrm{f}} J_{\mathrm{f}} \tag{4}$$

where q is the specific discharge; μ is the dynamic viscosity coefficient of the fluid; γ is the specific gravity of groundwater; J_f is the hydraulic gradient of fracture water flow; K_f is the permeability coefficient of the fracture.

From single-fracture seepage Eqs. (3) and (4), it can be known that the flow rate of the jth line element is:

$$q_j = \frac{\left(K_f\right)_j b_j \Delta H_j}{l_j} = R_j \Delta H_j \tag{5}$$

where K_f is the permeability coefficient of the fracture; b_j and l_j represent the width and length of the line element, respectively; ΔH_j denotes the head difference between the two ends of the j-line element.

The hydraulic conductivity of the j-line element is:

$$R_j = \frac{\gamma b_j^2}{12\mu} \bullet \frac{b_j}{l_j} \tag{6}$$

written in matrix form:

$$\mathbf{q} = \mathbf{R} \bullet \Delta\mathbf{H} \tag{7}$$

where $\Delta\mathbf{H} = \mathbf{A}^{\mathrm{T}}\mathbf{H}$, $\Delta\mathbf{H}$ is the column vector representing the head difference between the two ends of the line element, $\Delta\mathbf{H} = (\Delta H_1, \Delta H_2), \ldots, \Delta H_M)^{\mathrm{T}}$, $\mathbf{A}$ is the aggregation matrix reflecting the relationship between line elements and nodes in the fracture network, and $\mathbf{H}$ is the vector nodal heads; $\mathbf{q} = (q_1, q_2, \ldots, q_M)^{\mathrm{T}}$; $\mathbf{R} = \mathrm{diag}(R_1, R_2, \ldots, R_M)$.

By combining Eqs. (2) and (7), the final seepage solution formula for the DFN model can be obtained:

$$\left(\mathbf{A}\mathbf{R}\mathbf{A}^{\mathrm{T}}\right)\mathbf{H} = \mathbf{Q} \tag{8}$$

Mathematical model of water flow in a 2D continuous medium

The EPM model depicts fractured rock mass as a continuum seepage medium, and equally distributes fracture fluid in the whole rock mass; it considers fractured rock mass as a seepage medium with a symmetric permeability tensor (Chen et al. 2021a, b; Zhang et al. 2017). The 2D steady seepage in a saturated medium, based on Darcy's law, can be expressed as:

$$\frac{\partial}{\partial x} = \left(T_x \frac{\partial h}{\partial x}\right) + \frac{\partial}{\partial y}\left(T_y \frac{\partial h}{\partial y}\right) + W = 0 \tag{9}$$

where T_x and T_y are the transmissivities in the x and y directions; $h = h(x, y)$ is the head function; W represents the source-sink term per element area.

For the Neumann boundary Γ_2, the inflow or outflow per unit length on this boundary is known, and there are flow boundary conditions:

$$K_n \frac{\partial h}{\partial n}|_{\Gamma_2} = q(x, y) \tag{10}$$

where n is the external normal direction of Γ_2; $q(x, y)$ is the known flow rate. If the boundary is impermeable, then $q = 0$.

The solution to the initial-boundary value problem of seepage partial differential equations can be transformed into finding the extremal function of a certain functional. Therefore, solving Eq. (9) is equivalent to finding the minimal function of the following functional:

$$I(h) = \iint_{\Omega} \left\{ \frac{1}{2}\left[K_x\left(\frac{\partial h}{\partial x}\right)^2 + K_y\left(\frac{\partial h}{\partial y}\right)^2\right]\right\} \mathrm{d}x\mathrm{d}y + \int_{\Gamma_2} qh\mathrm{d}\Gamma \tag{11}$$

The seepage area Ω is discretized and divided into m disjoint units e, each unit contains M nodes, and the interpolation function is N_i, thus the head expression of the unit from any point is:

$$h = \sum_{i=1}^{M} N_i h_i \tag{12}$$

The seepage area Ω is decomposed into the sum of individual elements, and the boundary Γ_1 is decomposed into the sum of line elements, resulting in:

$$I(h) = \sum_{e=1}^{m} I^e(h) = \sum_{e=1}^{m} \iint_{e} \left\{ \frac{1}{2}\left[K_x\left(\frac{\partial h}{\partial x}\right)^2 + K_y\left(\frac{\partial h}{\partial y}\right)^2\right]\right\} \mathrm{d}x\mathrm{d}y + \int_{\Gamma_1} qh\mathrm{d}\Gamma \tag{13}$$

By substituting Eq. (12) into Eq. (13), $I(h)$ becomes a function of the hydraulic heads at each node. The sought function h should be the minimal function of the functional $I(h)$; therefore, it must satisfy:

$$\frac{\partial I}{\partial h_i} = \sum_{e=1}^{m} \frac{\partial I^e}{\partial h_i} = 0 \tag{14}$$

If the functional I is a quadratic function of h and its derivatives, then the functional I^e for any element e is also quadratic. Consequently, the solution equations are transformed into:

$$\mathbf{K}\mathbf{h} = \mathbf{F} \tag{15}$$

where $\mathbf{F}$ is a known constant term; The expression for an individual element in matrix $\mathbf{K}$ is as follows:

$$K_{ij}^{e} = \iint_{e} \left(K_x \frac{\partial N_i}{\partial x} \frac{\partial N_j}{\partial x} + K_y \frac{\partial N_i}{\partial y} \frac{\partial N_j}{\partial y} \right) \mathrm{d}x\mathrm{d}y \tag{16}$$

The corresponding relationship between elements in the whole conductivity matrix and elements in the unit conductivity matrix is as follows:

$$K_{ij} = \sum_{k=1}^{m_i} K_{ij}^{e_k} \tag{17}$$

where m_i is the number of units with common nodes i, j. Because there are few related nodes in each node, the overall conductivity matrix is a highly sparse symmetrical matrix.

In Eq. (15), the vector at the right end of the medium number is also obtained by superimposing the vector at the right end of the unit. The calculation formula of each element in the vector at the right end of the unit is:

$$F_i^e = \iint_e wN_i \mathrm{d}\Omega + \int_{\Gamma_1} qN_i \mathrm{d}\Gamma \tag{18}$$

where w is the amount of infiltration or evaporation water; q is the inflow per unit area of the boundary.

Solution of the 2D discrete fracture-matrix model

In order to solve the problem of 2D steady flow in areas where continuous media and fractured media are adjacent to each other, this study uses the discrete fracture-matrix coupling flow method (Fig. 1). The key of the method is, firstly, the corresponding integral seepage matrices of fractured media and continuous media in the whole seepage area are established respectively, and then based on the principle of equal water head and flow balance of the common nodes of the two types of media, the integral seepage matrix of the whole seepage area is formed for further finite element analysis, which is actually an integral solution method (Guo et al. 2023; Hyman et al. 2022; Mi et al. 2017).

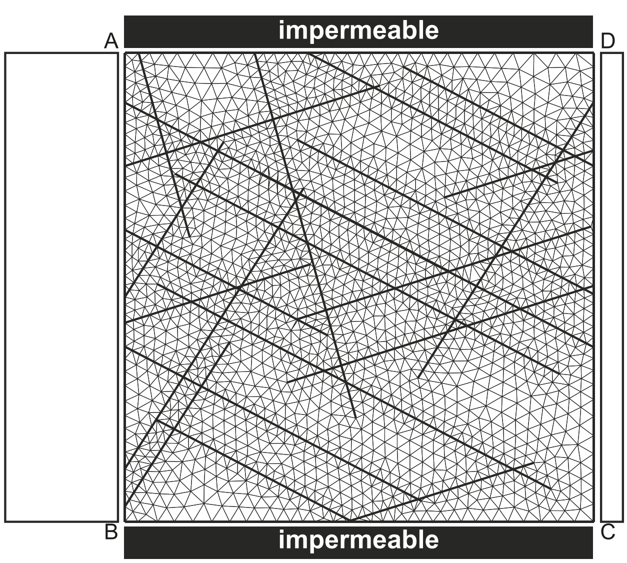

Fig. 1 Schematic diagram of a discrete fracture-matrix model

According to the seepage theory of fracture network in section 'Mathematical model of water flow in 2D discrete fractures', the steady flow equation of a 2D fracture network can be written as follows:

$$\mathbf{ARA}^{\mathrm{T}}\mathbf{h} = \mathbf{Q} \tag{19}$$

where $\mathbf{A}$ is the aggregation matrix; $\mathbf{R}$ is the coefficient matrix of hydraulic conductivity of fracture; $\mathbf{h}$ is the node head; $\mathbf{Q}$ is the source-sink term.

Based on the Ritz finite element method, the process of fracture seepage is the same as that of continuous medium seepage theory, described in section 'Mathematical model of water flow in a 2D continuous medium'. Each fracture segment is regarded as a line element to discretize the fracture seepage area. If the two ends of line element j are node i and node $i+1$, respectively, there is an elemental seepage matrix as follows:

$$\mathbf{K}^j = \frac{K_j}{l_j} \begin{bmatrix} 1 & -1 \\ -1 & 1 \end{bmatrix} \tag{20}$$

$$K_j = \frac{\gamma b^3}{12\mu} \tag{21}$$

For line element j, there is an equation as follows:

$$\mathbf{K}^j \mathbf{h}^j = \begin{bmatrix} \frac{\gamma b_j^3}{12\mu l_j} & -\frac{\gamma b_j^3}{12\mu l_j} \\ -\frac{\gamma b_j^3}{12\mu l_j} & \frac{\gamma b_j^3}{12\mu l_j} \end{bmatrix} \begin{Bmatrix} h_i \\ h_{i+1} \end{Bmatrix} = \begin{Bmatrix} Q_i \\ Q_{i+1} \end{Bmatrix} \tag{22}$$

where Q_i and Q_{i+1} are the known flow rates of node i and node $i+1$, respectively.

The overall permeability matrix ($\mathbf{K}$) is obtained by superimposing all element permeability matrices, and finally, the finite element equation is:

$$\mathbf{Kh} = \mathbf{Q} \tag{23}$$

And there is:

$$\mathbf{K} = \mathbf{ARA}^{\mathrm{T}} \tag{24}$$

when coupling the fractured system and the continuous medium system, the fractured medium can be discretized by the line element, and the continuous medium can be discretized by the triangular element (Fig. 2). All nodes are numbered uniformly to obtain a permeability matrix of every triangular element. These matrices are assembled together according to node connection relationships to form

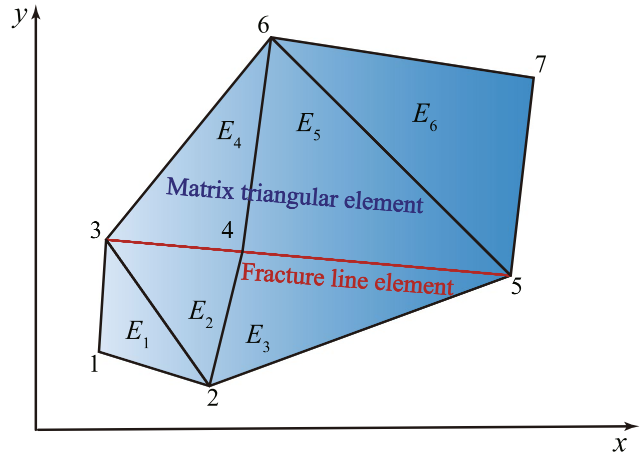

Element number	Node number		
	i	*j*	*k*
1	1	2	3
2	2	4	3
3	2	5	4
4	3	4	6
5	4	5	6
6	5	7	6

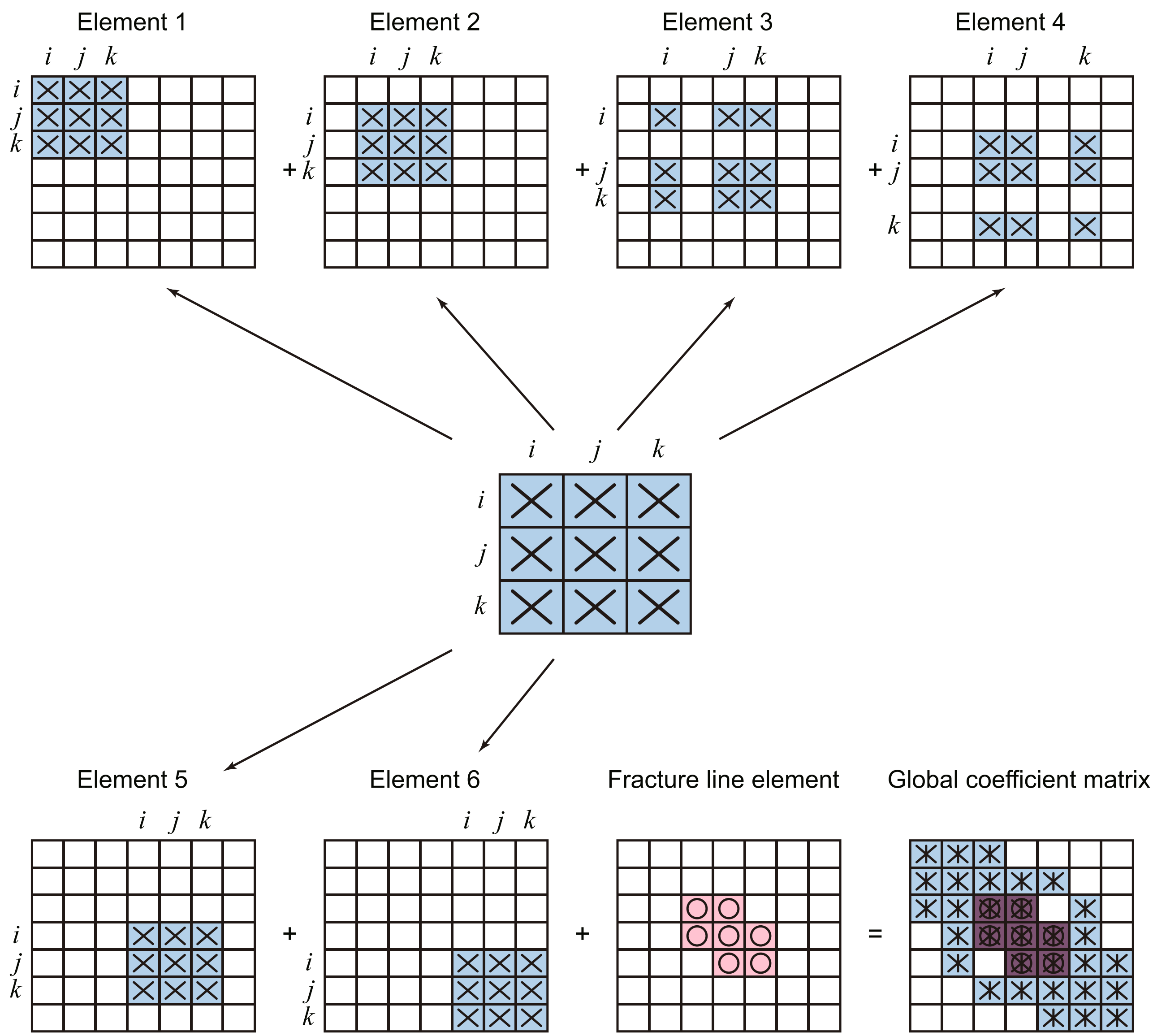

Fig. 2 Schematic diagram of the fracture and matrix spatial discretization

the overall permeability matrix, after which the boundary conditions are added to solve the seepage flow.

Suitability evaluation of the EPM model

For a study area with known fracture geometry parameters and rock matrix permeability, the DFM model can be used to solve the hydraulic head of each node in the study area, and the DFM simulation results are taken as the reference value of the hydraulic head in the study area. Accordingly, the EPM model is used to calculate the hydraulic head of each node of the same study area. Finally, comparing the simulation results of the EPM model with those of the DFM model, the hydraulic head error of each node from the EPM model simulation can be solved, and the error is used to evaluate the suitability of the EPM model.

When utilizing the EPM model to solve for the hydraulic head of each node in the fractured rock mass, the fractured rock mass is characterized as a continuum seepage medium, equally distributing the water in the whole rock mass. The aquifer is assumed to be homogeneous, thus the hydraulic head at any position in the study area can be obtained by:

$$H_p = H_{b1} + \frac{l_{pAB}}{l_{AD}}\left(H_{b2} - H_{b1}\right) \tag{25}$$

where H_p is the hydraulic head at any position p in the study area, l_{pAB} is the distance from position p in the study area to boundary AB, l_{AD} is the AD boundary length, and H_{b1} and H_{b2} are the hydraulic heads at the left and right boundaries, respectively, of the study area.

After obtaining the simulation results of the EPM model and the DFM model in the study area, this study mainly uses three calculation methods to quantitatively evaluate the influence of fracture aperture and rock matrix permeability on the suitability of the EPM model, including the commonly used mean absolute error (MAE) and root mean square error (RMSE) values and the suitable rate of the EPM model proposed to express the suitability of the EPM model more intuitively.

In statistics, the MAE is the average value of the absolute errors. It is a measure of the errors between pairs of observations expressing the same phenomenon, which can suitably reflect the actual situation of the prediction errors. The calculation formula is as follows:

$$\text{MAE} = \frac{\sum_{i=1}^{m}\left|\text{predicted}_i - \text{actual}_i\right|}{m} \tag{26}$$

The RMSE is a statistical metric commonly used to quantify the deviation between observed values and true values. It is calculated as the square root of the mean of the squared differences between observed and true values, divided by the number of observations m. The formula for calculating RMSE is as follows:

$$\text{RMSE} = \sqrt{\frac{1}{m}\sum_{i=1}^{m}\left(\text{predicted}_i - \text{actual}_i\right)^2} \tag{27}$$

The MAE is conceptually simpler and easier to explain than the RMSE. It is just the average absolute vertical or horizontal distance between each point in the scatter plot and the $y = x$ line. In addition, the contribution of each error to MAE is proportional to the absolute value of the error. This is in contrast to RMSE which involves squaring the error; thus, some larger errors will make RMSE increase more than MAE.

To provide a more intuitive and straightforward evaluation of the EPM model's suitability, the suitable rate was utilized to assess its performance. The relative error is calculated as follows:

$$\delta_i = \frac{H_i' - H_i}{H_{\max} - H_{\min}} \tag{28}$$

where δ_i represents the relative error at node i, while H_i' and H_i correspond to the hydraulic head values at node i obtained from the DFM and EPM models, respectively. Additionally, $H_{\max}$ denotes the maximum hydraulic head value in the study area, and $H_{\min}$ represents the minimum water head value. Based on the relative error, a criterion was established to determine the suitability of the EPM model at each node. If the relative error at node i is less than or equal to 0.15, the EPM model simulation results are considered satisfactory. Conversely, if the relative error exceeds 0.15, the EPM model's performance is deemed inadequate at that particular node. This can be expressed as:

$$e_i = \begin{cases} 1, \delta_i \le 0.15 \\ 0, \delta_i > 0.15 \end{cases} \tag{29}$$

where e_i represents the suitability of the EPM model at node i. A value of 1 indicates that the EPM model is suitable for that node, while a value of 0 suggests that the EPM model is unsuitable. To assess the overall suitability of the EPM model, the suitable rate is computed by dividing the number of suitable nodes by the total number of nodes:

$$\eta = \frac{\sum_{i=1}^{N_t} e_i}{N_t} \tag{30}$$

where η denotes the suitability of the EPM model, ranging from 0 to 1. The η closer to 0 indicates poor suitability, while the η closer to 1 implies better suitability. N_t represents the total number of nodes in the study area.

By systematically varying the fracture aperture and matrix permeability in the study area, different fracture networks are generated, allowing for the suitability of the EPM model for each network to be calculated, thus enabling an exploration of the impact of fracture aperture and matrix permeability on the EPM model's suitability.

Numerical model setup

This study employed a numerical simulation method to obtain simulated heads, enabling the evaluation of the EPM model's suitability. The parameters in the numerical model were primarily determined based on the investigation results from the Three Gorges Dam Project in China (Wang et al. 2020a, b). The statistical characteristics of four fracture groups in the area are presented in Table 1. To model the fracture trace length and aperture, a lognormal distribution was assumed following the work of Tonon and Chen (2007). Additionally, the fracture orientation probability distribution was considered to follow a normal distribution based on the studies by Chen et al. (2008) and Ni et al. (2017). Fracture density was treated as constant, defined as the total number of fractures divided by a given area.

In this study, a 2D fracture network model with dimensions of 20×20 m was generated using the Monte Carlo method based on fracture geometric parameters. It is worth noting that boundary conditions play a crucial role in investigating the seepage behavior of fractured rock masses. This study defined the left and right boundaries as constant-head boundaries, with hydraulic heads set to 2 and 0 m, respectively. The upper and lower boundaries were considered impermeable, allowing water to enter from the left boundary and exit from the right boundary. The fluid flow was assumed to be steady.

To solve for the head values at each node of the fracture network, MATLAB software was used, taking into account the generated computational domain, boundary conditions, fracture distribution, and parameters. As the fracture network generated through the Monte Carlo simulation method exhibits certain randomness, the operations were repeated for all models 200 times (realizations). This approach was adopted to reduce random errors while considering the trade-off between computational burden and accuracy requirements.

The influence of the fracture aperture on the permeability of fractured rock mass was quantitatively studied. Nine fracture apertures were set in this study (Table 2), which was modified by the classification standard of the fracture aperture in ISRM 1978 (Mechanics 1978). Other geometric parameters of fractures were controlled, and the permeability of the rock matrix was set to 0 m/s, which means that the matrix is impermeable. These DFN models were used to quantitatively analyze the influence of fracture aperture on the permeability of fractured rock mass when the rock matrix permeability is neglected.

In previous studies, the matrix permeability of fractured rock mass is often neglected, which often leads to a larger error in judgment on the suitability of the EPM model. The permeability of the rock matrix and fracture aperture control the overall permeability of fractured rock mass at the same time; thus, the influence of both of them on the suitability of the EPM model was studied (Chen et al. 2021a, b). According to Table 2, nine different fracture apertures were selected to build fracture network models (Fig. 3), while the other geometric parameters of fractures are kept constant. As shown in Fig. 4, the matrix permeability of the fractured rock mass gradually increases from 0 to 0.01 m/s, and 12 different matrix permeability values of fractured rock mass were used for the numerical simulation. Totally, 108 fracture network models with different parameters were generated, and 21,600 numerical calculations were performed. The DFM model was used to quantitatively study the influence of fracture aperture and rock matrix permeability on the suitability of the EPM model.

Table 2 Classification standard of fracture aperture (modified by ISRM,1978)

Description	Aperture (mm)
Very tight	0.10
Tight 1	0.17
Tight 2	0.25
Partly open 1	0.37
Partly open 2	0.50
Open 1	1.50
Open 2	2.50
Moderately wide	6.25
Wide	10.00

Table 1 Geometric parameters of fracture for generating the initial DFM model

Fracture group	Dip angle (°)		Length (m)		Aperture (mm)		Density (per m^2)
	Mean	Variance	Mean	Variance	Mean	Variance	
1	332.5	7.5	5.63	0.45	0.27	0.13	0.35
2	17.5	6.5	4.35	0.35	0.27	0.13	0.17
3	57.5	13.0	3.82	0.28	0.27	0.13	0.11
4	285.5	13.5	4.54	0.22	0.27	0.13	0.08

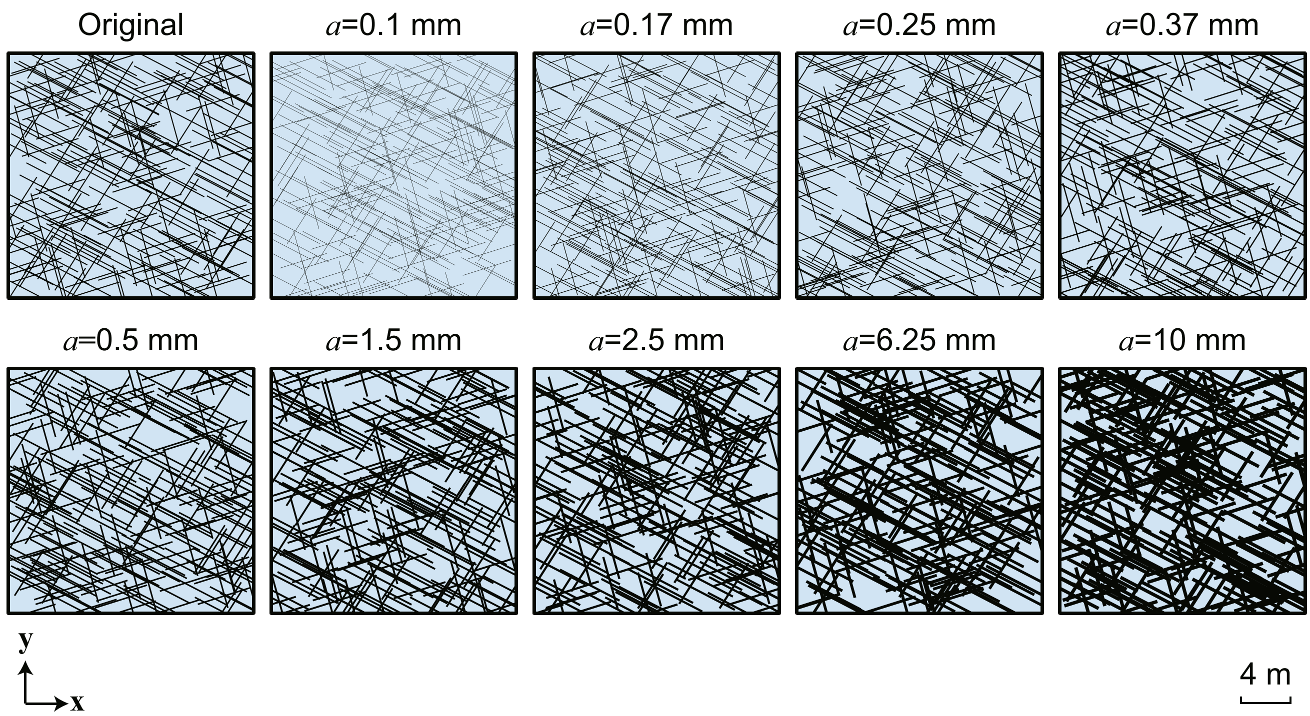

Fig. 3 2D DFM models with nine different apertures; 'Original' refers to the original fracture aperture, set at a value of 0.27 mm

Results and discussion

Simulation results of the DFN model

The DFN model was used to explore the influence of fracture aperture on the permeability of fractured rock mass when the matrix permeability is ignored. The hydraulic conductivity K is the smallest when the fracture aperture is 0.1 mm ($K = 9.086\times10^{-7}$ m/s), and the largest K is 0.9086 m/s when the fracture aperture is 10 mm. The overall K of fractured rock mass increases exponentially with the increase of fracture aperture, and K is proportional to the third power of the fracture aperture.

If the matrix permeability of fractured rock mass was to be ignored, the DFN model was used to solve the head of each node in the study area, and the simulation results were taken as the reference value of the head in the study area. The EPM model was used to obtain the hydraulic head results of each node in the study area. Finally, by comparing the EPM model simulation results with the DFN simulation results, the hydraulic head error of each node in the study area was calculated to evaluate the suitability of the EPM model. The three calculation methods were mainly used to quantitatively evaluate the influence of fracture aperture on the suitability of the EPM model, including the commonly used MAE and RMSE values and the suitability of the ECM model. These models were all run 200 times to reduce the error caused by randomness. The results show that, when the rock matrix permeability was neglected, with the increase of fracture aperture, the MAE value was 0.1252 m, the RMSE value was 0.1673 m, and the suitability of the EPM model was 0.8783. Under the condition of ignoring the permeability of rock matrix and keeping other fracture geometric parameters unchanged, the change of fracture aperture has no effect on the water head distribution in fractured rock mass, and thus does not affect the suitability of the EPM model.

Simulation results of the DFM model

The DFM model was used to quantitatively study the influence of fracture aperture and rock matrix permeability on the suitability of the EPM model. The results were shown in Fig. 5. With the fracture aperture increasing gradually, the MAE tends to increase gradually. When the fracture aperture increases to a certain limit, the MAE value begins to increase, and finally reaches the maximum value of 0.1252. When the fracture aperture increases beyond this limit, the MAE value will not change. RMSE value keeps the same trend as the MAE value; it gradually increases with the fracture aperture. When the fracture aperture increases to a certain limit, the RMSE value begins to increase and finally reaches the maximum value of 0.1673, and then increases the fracture aperture, and the RMSE value does not change. The matrix permeability of fractured rock mass mainly affects the starting point and endpoint of increases of MAE and RMSE. The influence of fracture aperture on the suitability of the EPM model is emphatically analyzed considering the permeability of rock

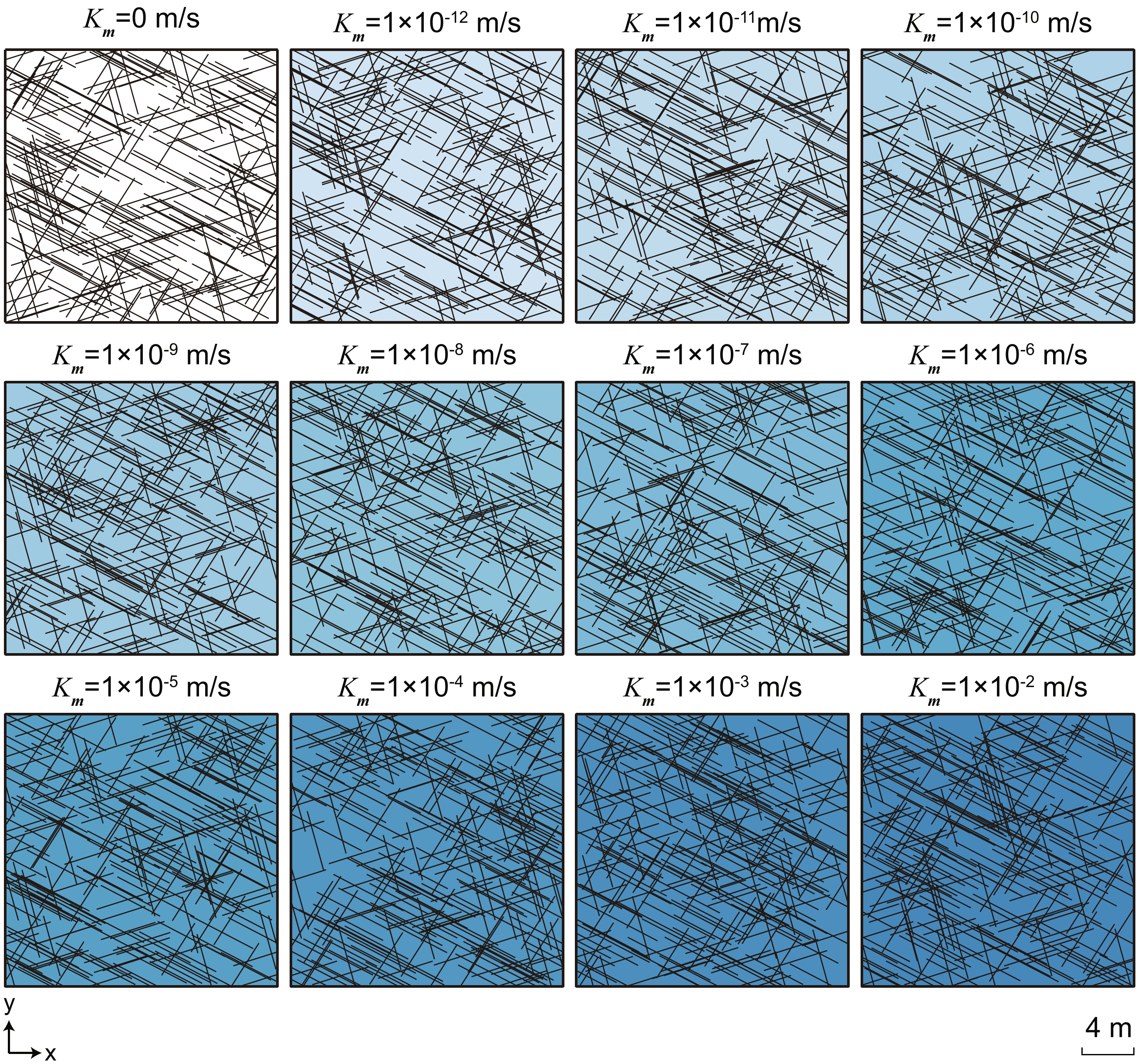

Fig. 4 Twelve 2D DFM models with different rock matrix permeability of fractured rock mass

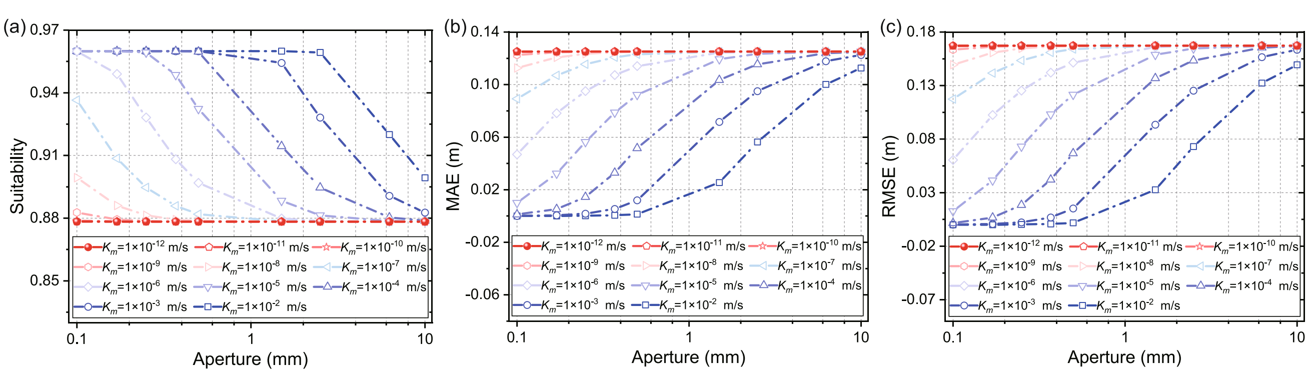

Fig. 5 Influence of fracture aperture on the suitability of the EPM model: **a** suitability value, **b** MAE value, **c** RMSE value

matrix. Generally, when the permeability coefficient of rock matrix is small, the fracture aperture has little influence on the suitability of the EPM model. When the matrix permeability coefficient is relatively larger, the suitability of the EPM model shows a decreasing trend with the increase of fracture aperture, gradually decreasing from the maximum of 0.9599 to finally 0.8793. When the fracture aperture is relatively smaller, the matrix permeability of fractured rock mass significantly affects the suitability of the EPM model. The greater the permeability, the greater the suitability of the EPM model. The matrix permeability also affects the inflection point where the suitability decreases, and the end point where the suitability tends to be stable (Fig. 5a). With the increase of matrix permeability, the inflection point of decrease will be delayed—in other words, only when the fracture aperture is larger will the fracture aperture affect the suitability of the EPM model. When the permeability of the rock matrix is smaller, the change of fracture aperture will not affect the suitability of the EPM model, which is consistent with the characteristics that the suitability of the EPM model remains unchanged with the increase of fracture aperture when the permeability of rock matrix is ignored (section 'Simulation results of the DFN model'). The change trends of RMSE and MAE with aperture and matrix permeability are similar (Fig. 5b,c), which are generally reversed compared with the suitability change trend.

This research also focuses on the influence of the permeability of the rock matrix on the suitability of the EPM model, which is widely ignored by many scholars. The research results are plotted in Fig. 6. With the gradual increase of the permeability of rock matrix, the suitability of the EPM model gradually increases. No matter what the fracture aperture values are, the suitability of the EPM model gradually increases with matrix permeability, starting from the minimum of 0.8783 and finally reaching 0.9599, then tends to be stable. Different fracture apertures have different starting points and end points of the change curve. With the increase of fracture aperture, the starting point and end point will be delayed correspondingly. The trends of MAE and RMSE are consistent. With the increase of matrix permeability, the values of MAE and RMSE gradually decrease, and different fracture apertures have different starting points and end points of curve decline. Using suitability rates, MAE, and RMSE methods to study the influence of permeability of rock matrix on the suitability of the EPM model, the results are very similar, but the suitability rate of the EPM model will reach the stable point faster than the MAE and RMSE.

Suitability evaluation of the EPM model

Curve fitting is carried out based on the influence of the permeability of rock matrix on the suitability of the EPM model. The results are shown in Fig. 7. It can be found that the fitting results of the suitability vs. different fracture apertures have the same form, and the fitting curve perfectly conforms to the Boltzmann formula (Hashemireza et al. 2023):

$$y = \frac{A_1 - A_2}{1 + e^{(x-x_0)/w}} + A_2 \tag{31}$$

The significance of each parameter in the fitted formula was further explored. Among them, A_1 is the lowest value of the curve. Regardless of the variations in fracture apertures, A_1 consistently remains at 0.8783, a value that is also indicative of the suitability rate of the EPM model when the permeability of the rock matrix is ignored. As mentioned in section 'Simulation results of the DFM model', this value is not affected by the fracture aperture. A_2 is the highest value of the curve, remaining constant at 0.9599 across different fracture apertures, indicating that once the matrix permeability increases to a certain limit, the influence of the existence of fractures on the permeability of fractured rock mass is minimal and can be approximately ignored. The permeability of the fractured rock mass can be approximately considered equal everywhere, and then the EPM model can be perfectly used for fractured rock mass. In the case of different fracture apertures, w in the fitting formula fluctuates little and can be approximately regarded as a constant, which represents the changing intensity of the curve when the suitability increases the most. With different fracture apertures, the absolute value

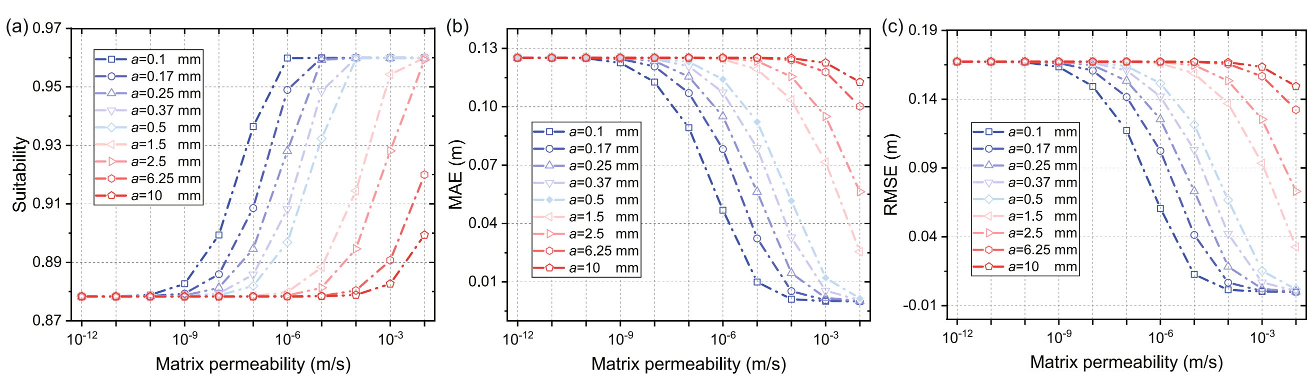

Fig. 6 Influence of matrix permeability on the suitability of the EPM model: **a** suitability value, **b** MAE value, **c** RMSE value

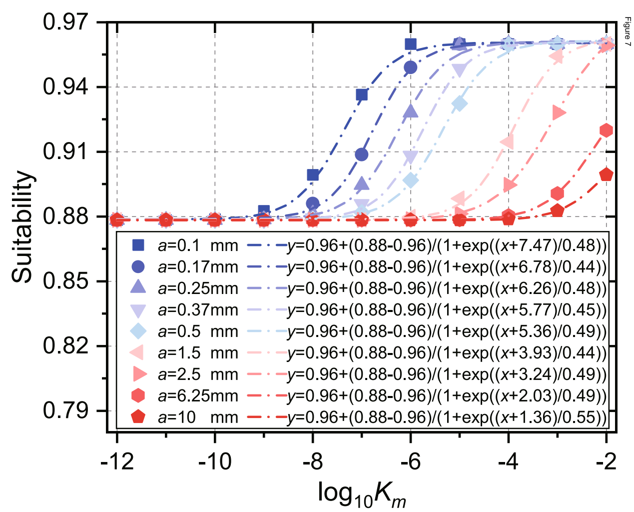

Fig. 7 Fitting curve of influence of the matrix permeability on the suitability of the EPM model

of parameter x_0 changes to become larger, and it reduces with fracture aperture increase. This study focused on the influencing factors of changing x_0. The results show that x_0 is related to the rock permeability when the matrix permeability of the fractured rock mass is ignored. As shown in Fig. 8, the fitting parameter x_0 is proportional to $\log_{10}K$. Here, K represents the overall permeability K of the fractured rock mass obtained when not considering matrix permeability. In this way, when evaluating the suitability of the EPM model for a site, one can consider the influence of fracture matrix permeability on the EPM model, or consider fracture matrix permeability to modify the suitability of the EPM model according to the existing site conditions. Firstly, without considering the permeability of rock matrix, the suitability of the EPM model for this site is A_1, and the rock permeability K can be obtained at the same time; A_2 and w are fixed values, which are roughly 1 and 0.478 respectively. Then, x_0 is calculated according to the formula with the rock permeability K, and the influence curve of matrix permeability of fractured rock mass on the suitability of the EPM model is combined to quantitatively evaluate the influence of matrix permeability of fractured rock mass on the suitability of the EPM model.

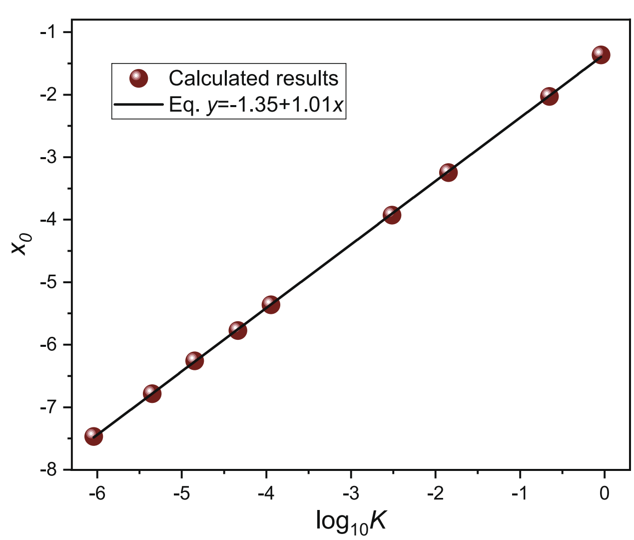

Fig. 8 Relationship between the fitting parameter x_0 and permeability of the fractured rock mass when matrix permeability of fractured rock mass is ignored

Conclusions

In this study, the influence of fracture aperture and matrix permeability of fractured rock mass on the suitability of the EPM model was explored by the numerical simulation method. By keeping the geometric parameters unchanged and by changing the related parameters of fracture aperture and matrix permeability of the fractured rock mass, the fracture network is generated by the Monte Carlo simulation method and hydraulic head is solved by the DFM model. A total of 108 sets of EPM models were built to analyze the influence of comprehensive fracture aperture and matrix permeability of fractured rock mass on the suitability of this model. To reduce the influence of randomness on the results, 200 random simulations as well as a total of 21,600 numerical simulation experiments were carried out for each model.

The results indicate that when the matrix permeability of fractured rock mass is neglected, the overall hydraulic conductivity K of the fractured rock mass increases exponentially with the increase of fracture aperture, and K is proportional to the third power of fracture aperture. With the increase of fracture aperture, MAE, RMSE and the suitability of the EPM models remain unchanged, which is to say, that the change of fracture aperture does not affect the suitability of the EPM model. Considering the combined influence of fracture aperture and matrix permeability of fractured rock mass on the suitability of the EPM model, with the increase of fracture aperture, the suitability of the EPM model tends to decrease, and the difference in matrix permeability of the fractured rock mass mainly affects the inflection point where the suitability decreases. With the increase of matrix permeability, the inflection point will be delayed. With the gradual increase of the matrix permeability of fractured rock mass, the suitability of the EPM model gradually increases, and different fracture apertures affect the starting point and end point of the curve. With the increase of fracture aperture, the starting point and end point will be delayed correspondingly. According to the influence of matrix permeability on the suitability of the EPM model, the curve-fitting result perfectly accords with the Boltzmann formula. When evaluating the suitability of the EPM model of a site, the influence of matrix permeability on the suitability of the EPM model can be quantitatively calculated.

The present study provides valuable insight into the influence of fractures and matrix on the suitability of the EPM method for addressing hydraulic-head-related hydrogeological issues in fractured geological media. While the effects of fracture aperture and matrix permeability were examined in this study, it is important to note that other fracture geometric parameters, such as uneven distribution and fracture roughness, were not comprehensively considered. Additionally, the study focused on a 2D fracture network, whereas in three-dimensional (3D) space, the complexities of water flow and transmission in fractured rock masses are amplified due to factors like fracture connectivity and spatial positioning. Therefore, it is essential to conduct further investigations to determine the suitability conditions of the EPM model in 3D space, accounting for a broader range of fracture geometric parameters.

Appendix: Nomenclature

Symbol	Description	Units
q	Unit width of discharge	L^2T^{-1}
Q	Source-sink term at fracture	L^2T^{-1}
N'	Degree of node i	
N	Number of nodes	
M	Number of line elements	
$\mathbf{A}$	An aggregation matrix reflecting the aggregation relationship between the line elements and nodes	
$\mathbf{q}$	$\mathbf{q}=(q_1,q_2,\ldots,q_N)^T$	L^2T^{-1}
$\mathbf{Q}$	$\mathbf{Q}=(Q_1,Q_2,\ldots,Q_N)^T$	L^2T^{-1}
μ	Dynamic viscosity coefficient of the fluid	$ML^{-1}T^{-1}$
γ	Specific gravity of groundwater	
J_f	Hydraulic gradient of fracture water flow	
b	Fracture width	L
V	Average velocity	LT^{-1}
K	Hydraulic conductivity	LT^{-1}
l	Fracture length	L
ΔH	Head difference	L
R_j	Hydraulic conductivity of the j line element	LT^{-1}
h	Head	L
$\mathbf{\Delta H}$	$\mathbf{\Delta H}=(\Delta H_1, \Delta H_2,\ldots,\Delta H_M)^T$	L
$\mathbf{R}$	$\mathbf{R}=\mathrm{diag}(R_1,R_2,\ldots,R_M)$	LT^{-1}
$\mathbf{H}$	$\mathbf{H}=(h_1, h_2,\ldots, h_M)^T$	L
W	Source-sink term	LT^{-1}
m_i	Number of units with common nodes i, j	
$\mathbf{K}$	Permeability coefficient matrix	LT^{-1}
$\mathbf{F}$	Known constant term matrix	L^2T^{-1}
w	Infiltration or evaporation water	LT^{-1}
m	Number of observations	
a	Aperture	L
δ_i	Relative error	
η	Suitability of the EPM model	

Acknowledgements The authors would like to acknowledge the editors and anonymous reviewers for their invaluable discussion and suggestions.

Funding This work was supported by the National Natural Science Foundation of China (Nos. U2267218 and 42072276).

Declarations

Conflict of interests The authors declare that they have no known competing financial interests or personal relationships that could have appeared to influence the work reported in this paper.

References

Applegate D, Appleyard P (2022) Capability for hydrogeochemical modelling within discrete fracture networks. Energies 15:6199. https://doi.org/10.3390/en15176199*10.3390/en15176199
Baghbanan A, Jing L (2008) Stress effects on permeability in a fractured rock mass with correlated fracture length and aperture. INT J Rock Mech Min 45:1320–1334. https://doi.org/10.1016/j.ijrmms.2008.01.015*10.1016/j.ijrmms.2008.01.015
Berrone S, Borio A, Vicini F (2019) Reliable a posteriori mesh adaptivity in discrete fracture network flow simulations. Comput Method Appl M 354:904–931. https://doi.org/10.1016/j.cma.2019.06.007*10.1016/j.cma.2019.06.007
Binda G, Pozzi A, Spanu D, Livio F, Trotta S, Bitonte R (2021) Integration of photogrammetry from unmanned aerial vehicles, field measurements and discrete fracture network modeling to understand groundwater flow in remote settings: test and comparison with geochemical markers in an Alpine catchment. Hydrogeol J 29:1203–1218. https://doi.org/10.1007/s10040-021-02304-4*10.1007/s10040-021-02304-4
Bisdom K, Bertotti G, Nick HM (2016) The impact of in-situ stress and outcrop-based fracture geometry on hydraulic aperture and upscaled permeability in fractured reservoirs. Tectonophysics 690:63–75. https://doi.org/10.1016/j.tecto.2016.04.006*10.1016/j.tecto.2016.04.006
Bosma S, Hajibeygi H, Tene M, Tchelepi HA (2017) Multiscale finite volume method for discrete fracture modeling on unstructured grids (MS-DFM). J Comput Phys 351:145–164. https://doi.org/10.1016/j.jcp.2017.09.032*10.1016/j.jcp.2017.09.032
Bou Jaoude I, Novakowski K, Kueper B (2022) Comparing heat and solute transport in a discrete rock fracture of variable aperture. J Hydrol 607:127496. https://doi.org/10.1016/j.jhydrol.2022.127496*10.1016/j.jhydrol.2022.127496
Chen SH, Feng XM, Isam S (2008) Numerical estimation of REV and permeability tensor for fractured rock masses by composite element method. Int J Numer Anal Met 32:1459–1477. https://doi.org/10.1002/nag.679*10.1002/nag.679
Chen M, Masum SA, Thomas HR (2022) 3D hybrid coupled dual continuum and discrete fracture model for simulation of CO_2 injection into stimulated coal reservoirs with parallel implementation. Int J Coal Geol 262:104103. https://doi.org/10.1016/j.coal.2022.104103*10.1016/j.coal.2022.104103
Chen Y, Yu H, Ma H, Li X, Hu R, Yang Z (2020) Inverse modeling of saturated-unsaturated flow in site-scale fractured rocks using the continuum approach: a case study at Baihetan Dam site, Southwest China. J Hydrol 584:124693. https://doi.org/10.1016/j.jhydrol.2020.124693*10.1016/j.jhydrol.2020.124693
Chen Y, Zeng J, Shi H, Wang Y, Hu R, Yang Z, Zhou C (2021a) Variation in hydraulic conductivity of fractured rocks at a dam foundation during operation. J Rock Mech Geotech 13:351–367. https://

doi.org/10.1016/j.jrmge.2020.09.008*10.1016/j.jrmge.2020.09.008
Chen Y, Zhou Z, Wang J, Zhao Y, Dou Z (2021b) Quantification and division of unfrozen water content during the freezing process and the influence of soil properties by low-field nuclear magnetic resonance. J Hydrol 602:126719. https://doi.org/10.1016/j.jhydrol.2021.126719*10.1016/j.jhydrol.2021.126719
Dodangeh A, Rajabi MM, Fahs M (2023) Combining harmonic pumping with a tracer test for fractured aquifer characterization. Hydrogeol J 31:371–385. https://doi.org/10.1007/s10040-023-02595-9*10.1007/s10040-023-02595-9
Dou Z, Sleep B, Mondal P, Guo Q, Wang J, Zhou Z (2018) Temporal mixing behavior of conservative solute transport through 2D self-affine fractures. Processes 6:158. https://doi.org/10.3390/pr6090158*10.3390/pr6090158
Dou Z, Sleep B, Zhan H, Zhou Z, Wang J (2019) Multiscale roughness influence on conservative solute transport in self-affine fractures. Int J Heat Mass Tran 133:606–618. https://doi.org/10.1016/j.ijheatmasstransfer.2018.12.141*10.1016/j.ijheatmasstransfer.2018.12.141
Feng S, Wang H, Cui Y, Ye Y, Liu Y, Li X, Wang H, Yang R (2020) Fractal discrete fracture network model for the analysis of radon migration in fractured media. Comput Geotech 128:103810. https://doi.org/10.1016/j.compgeo.2020.103810*10.1016/j.compgeo.2020.103810
Fu P, Johnson SM, Carrigan CR (2013) An explicitly coupled hydro-geomechanical model for simulating hydraulic fracturing in arbitrary discrete fracture networks. Int J Numer Anal Met 37:2278–2300. https://doi.org/10.1002/nag.2135*10.1002/nag.2135
Geetha Manjari K, Sivakumar Babu GL (2022) Reliability and sensitivity analyses of discrete fracture network based contaminant transport model in fractured rocks. Comput Geotech 145:104674. https://doi.org/10.1016/j.compgeo.2022.104674*10.1016/j.compgeo.2022.104674
Guo L, Fahs M, Koohbor B, Hoteit H, Younes A, Gao R, Shao Q (2023) Coupling mixed hybrid and extended finite element methods for the simulation of hydro-mechanical processes in fractured porous media. Comput Geotech 161:105575. https://doi.org/10.1016/j.compgeo.2023.105575*10.1016/j.compgeo.2023.105575
Hashemireza F, Sharafati A, Raziei T, Nazif S (2023) A double sigmoidal model for snow-rain phase separation. J Hydrol 617:129153. https://doi.org/10.1016/j.jhydrol.2023.129153*10.1016/j.jhydrol.2023.129153
He X, Sinan M, Kwak H, Hoteit H (2021) A corrected cubic law for single-phase laminar flow through rough-walled fractures. Adv Water Resour 154:103984. https://doi.org/10.1016/j.advwatres.2021.103984*10.1016/j.advwatres.2021.103984
Hu J, Ke H, Chen YM, Xu XB, Xu H (2021) Analytical analysis of the leachate flow to a horizontal well in dual-porosity media. Comput Geotech 134:104105. https://doi.org/10.1016/j.compgeo.2021.104105*10.1016/j.compgeo.2021.104105
Hu Y, Xu W, Zhan L, Zou L, Chen Y (2022) Modeling of solute transport in a fracture-matrix system with a three-dimensional discrete fracture network. J Hydrol 605:127333. https://doi.org/10.1016/j.jhydrol.2021.127333*10.1016/j.jhydrol.2021.127333
Huang N, Liu R, Jiang Y, Cheng Y (2021) Development and application of three-dimensional discrete fracture network modeling approach for fluid flow in fractured rock masses. J Nat Gas Sci Eng 91:103957. https://doi.org/10.1016/j.jngse.2021.103957*10.1016/j.jngse.2021.103957
Hyman JD, Dentz M (2021) Transport upscaling under flow heterogeneity and matrix-diffusion in three-dimensional discrete fracture networks. Adv Water Resour 155:103994. https://doi.org/10.1016/j.advwatres.2021.103994*10.1016/j.advwatres.2021.103994
Hyman JD, Sweeney MR, Gable CW, Svyatsky D, Lipnikov K, David Moulton J (2022) Flow and transport in three-dimensional discrete fracture matrix models using mimetic finite difference on a conforming multi-dimensional mesh. J Comput Phys 466:111396. https://doi.org/10.1016/j.jcp.2022.111396*10.1016/j.jcp.2022.111396
Jarrahi M, Moore KR, Holländer HM (2019) Comparison of solute/heat transport in fractured formations using discrete fracture and equivalent porous media modeling at the reservoir scale. Phys Chem Earth, Parts a/b/c 113:14–21. https://doi.org/10.1016/j.pce.2019.08.001*10.1016/j.pce.2019.08.001
Jia B, Xian C (2022) Permeability measurement of the fracture-matrix system with 3D embedded discrete fracture model. Petrol Sci 19:1757–1765. https://doi.org/10.1016/j.petsci.2022.01.010*10.1016/j.petsci.2022.01.010
Khafagy M, Dickson-Anderson S, El-Dakhakhni W (2022a) A rapid, simplified, hybrid modeling approach for simulating solute transport in discrete fracture networks. Comput Geotech 151:104986. https://doi.org/10.1016/j.compgeo.2022.104986*10.1016/j.compgeo.2022.104986
Khafagy M, El-Dakhakhni W, Dickson-Anderson S (2022b) Analytical model for solute transport in discrete fracture networks: 2D spatiotemporal solution with matrix diffusion. Comput Geosci-UK 159:104983. https://doi.org/10.1016/j.cageo.2021.104983*10.1016/j.cageo.2021.104983
Kim H, Onishi T, Chen H, Datta-Gupta A (2021) Parameterization of embedded discrete fracture models (EDFM) for efficient history matching of fractured reservoirs. J Petrol Sci Eng 204:108681. https://doi.org/10.1016/j.petrol.2021.108681*10.1016/j.petrol.2021.108681
Koohbor B, Fahs M, Hoteit H, Doummar J, Younes A, Belfort B (2020) An advanced discrete fracture model for variably saturated flow in fractured porous media. Adv Water Resour 140:103602. https://doi.org/10.1016/j.advwatres.2020.103602*10.1016/j.advwatres.2020.103602
Li B, Li Y, Zhao Z, Liu R (2019) A mechanical-hydraulic-solute transport model for rough-walled rock fractures subjected to shear under constant normal stiffness conditions. J Hydrol 579:124153. https://doi.org/10.1016/j.jhydrol.2019.124153*10.1016/j.jhydrol.2019.124153
Li Z, Zhang W, Zou X, Wu X, Illman WA, Dou Z (2023) An analytical model for solute transport in a large-strain aquitard affected by delayed drainage. J Hydrol 619:129380. https://doi.org/10.1016/j.jhydrol.2023.129380*10.1016/j.jhydrol.2023.129380
Liang Z, Wu N, Li Y, Li H, Li W (2019) Numerical study on anisotropy of the representative elementary volume of strength and deformability of jointed rock masses. Rock Mech Rock Eng 52:4387–4402. https://doi.org/10.1007/s00603-019-01859-9*10.1007/s00603-019-01859-9
Liu H, Zhao X, Tang X, Peng B, Zou J, Zhang X (2020) A Discrete fracture–matrix model for pressure transient analysis in multistage fractured horizontal wells with discretely distributed natural fractures. J Petrol Sci Eng 192:107275. https://doi.org/10.1016/j.petrol.2020.107275*10.1016/j.petrol.2020.107275
Liu Y, Wang Q, Chen J, Han X, Song S, Ruan Y (2021) Investigation of geometrical representative elementary volumes based on sampling directions and fracture sets. B Eng Geol Environ 80:2171–2187. https://doi.org/10.1007/s10064-020-02045-w*10.1007/s10064-020-02045-w
Lopes JAG, Medeiros WE, La Bruna V, de Lima A, Bezerra FHR, Schiozer DJ (2022) Advancements towards DFKN modelling: Incorporating fracture enlargement resulting from karstic dissolution in discrete fracture networks. J Petrol Sci Eng 209:109944. https://doi.org/10.1016/j.petrol.2021.109944*10.1016/j.petrol.2021.109944
Loyola AC, Pereira J, Cordão Neto MP (2021) General statistics-based methodology for the determination of the geometrical and mechanical representative elementary volumes of fractured media.

Rock Mech Rock Eng 54:1841–1861. https://doi.org/10.1007/s00603-021-02374-6*10.1007/s00603-021-02374-6

Luo W, Wang J, Wang L, Zhou Y (2020) An alternative BEM for simulating the flow behavior of a leaky confined fractured aquifer with the use of the semianalytical approach. Water Resour Res 56. https://doi.org/10.1029/2019WR026581*10.1029/2019WR026581

Ma L, Gao D, Qian J, Han D, Xing K, Ma H, Deng Y (2023a) Multiscale fractures integrated equivalent porous media method for simulating flow and solute transport in fracture-matrix system. J Hydrol 617:128845. https://doi.org/10.1016/j.jhydrol.2022.128845*10.1016/j.jhydrol.2022.128845

Ma L, Han D, Qian J, Gao D, Ma H, Deng Y, Hou X (2023b) Numerical evaluation of the suitability of the equivalent porous medium model for characterizing the two-dimensional flow field in a fractured geologic medium. Hydrogeol J 31:913–930. https://doi.org/10.1007/s10040-023-02627-4*10.1007/s10040-023-02627-4

Mechanics IISF (1978) Suggested methods for the quantitative description of discontinuities in rock masses. Document No. 4, Commission on Standardization of Laboratory and Field Tests. Int J Rock Mech Min Sci Geomech Abst 15:319–368

Mi L, Jiang H, Li J, Li T, Tian Y (2014) The investigation of fracture aperture effect on shale gas transport using discrete fracture model. J Nat Gas Sci Eng 21:631–635. https://doi.org/10.1016/j.jngse.2014.09.029*10.1016/j.jngse.2014.09.029

Mi L, Yan B, Jiang H, An C, Wang Y, Killough J (2017) An enhanced discrete fracture network model to simulate complex fracture distribution. J Petrol Sci Eng 156:484–496. https://doi.org/10.1016/j.petrol.2017.06.035*10.1016/j.petrol.2017.06.035

Mortazavi SMS, Pirmoradi P, Khoei AR (2022) Numerical simulation of cold and hot water injection into naturally fractured porous media using the extended–FEM and an equivalent continuum model. Int J Numer Anal Met 46:617–655. https://doi.org/10.1002/nag.3314*10.1002/nag.3314

Ni P, Wang S, Wang C, Zhang S (2017) Estimation of REV Size for fractured rock mass based on damage coefficient. Rock Mech Rock Eng 50:555–570. https://doi.org/10.1007/s00603-016-1122-x*10.1007/s00603-016-1122-x

Pham KT, Falta RW (2022) Use of semi-analytical and dual-porosity models for simulating matrix diffusion in systems with parallel fractures. Adv Water Resour 164:104202. https://doi.org/10.1016/j.advwatres.2022.104202*10.1016/j.advwatres.2022.104202

Qi-Zhen D, Xue-Mei W, Jing B, Qiang Z (2012) An equivalent medium model for wave simulation in fractured porous rocks. Geophys Prospect 60:940–956. https://doi.org/10.1111/j.1365-2478.2011.01027.x*10.1111/j.1365-2478.2011.01027.x

Rong G, Peng J, Wang X, Liu G, Hou D (2013) Permeability tensor and representative elementary volume of fractured rock masses. Hydrogeol J 21:1655–1671. https://doi.org/10.1007/s10040-013-1040-x*10.1007/s10040-013-1040-x

Salimzadeh S, Grandahl M, Medetbekova M, Nick HM (2019) A novel radial jet drilling stimulation technique for enhancing heat recovery from fractured geothermal reservoirs. Renew Energ 139:395–409. https://doi.org/10.1016/j.renene.2019.02.073*10.1016/j.renene.2019.02.073

Scanlon BR, Mace RE, Barrett ME, Smith B (2003) Can we simulate regional groundwater flow in a karst system using equivalent porous media models? Case study, Barton Springs Edwards aquifer, USA. J Hydrol 276:137–158. https://doi.org/10.1016/S0022-1694(03)00064-7*10.1016/S0022-1694(03)00064-7

Song J, Dong M, Koltuk S, Hu H, Zhang L, Azzam R (2018) Hydro-mechanically coupled finite-element analysis of the stability of a fractured-rock slope using the equivalent continuum approach: a case study of planned reservoir banks in Blaubeuren, Germany. Hydrogeol J 26:803–817. https://doi.org/10.1007/s10040-017-1694-x*10.1007/s10040-017-1694-x

Su Y, Huang Y, Shen H, Jiang Y, Zhou Z (2022) An analytical method for predicting the groundwater inflow to tunnels in a fractured aquifer. Hydrogeol J 30:1279–1293. https://doi.org/10.1007/s10040-022-02485-6*10.1007/s10040-022-02485-6

Sweeney MR, Gable CW, Karra S, Stauffer PH, Pawar RJ, Hyman JD (2020) Upscaled discrete fracture matrix model (UDFM): an octree-refined continuum representation of fractured porous media. Computat Geosci 24:293–310. https://doi.org/10.1007/s10596-019-09921-9*10.1007/s10596-019-09921-9

Ţene M, Bosma SBM, Al Kobaisi MS, Hajibeygi H (2017) Projection-based embedded discrete fracture model (pEDFM). Adv Water Resour 105:205–216. https://doi.org/10.1016/j.advwatres.2017.05.009*10.1016/j.advwatres.2017.05.009

Tonon F, Chen S (2007) Closed-form and numerical solutions for the probability distribution function of fracture diameters. Int J Rock Mech Min 44:332–350. https://doi.org/10.1016/j.ijrmms.2006.07.013*10.1016/j.ijrmms.2006.07.013

Wang L, Cardenas MB, Zhou JQ, Ketcham RA (2020a) The complexity of nonlinear flow and non-Fickian transport in fractures driven by three-dimensional recirculation zones. J Geophys Res: Solid Earth 125 https://doi.org/10.1029/2020JB020028*10.1029/2020JB020028

Wang X, Jiang Y, Liu R, Li B, Wang Z (2020b) A numerical study of equivalent permeability of 2D fractal rock fracture networks. Fractals 28:2050014. https://doi.org/10.1142/S0218348X20500140*10.1142/S0218348X20500140

Wang L, Golfier F, Tinet A, Chen W, Vuik C (2022a) An efficient adaptive implicit scheme with equivalent continuum approach for two-phase flow in fractured vuggy porous media. Adv Water Resour 163:104186. https://doi.org/10.1016/j.advwatres.2022.104186*10.1016/j.advwatres.2022.104186

Wang L, Zheng L, Singh K, Wang T, Liu-Zeng J, Xu S, Chen X (2022b) The effective pore volume of multiscale heterogenous fracture-porous media systems derived from the residence time of an inert tracer. J Hydrol 610:127839. https://doi.org/10.1016/j.jhydrol.2022.127839*10.1016/j.jhydrol.2022.127839

Wei S, Jin Y, Xia Y (2020) Predict the mud loss in natural fractured vuggy reservoir using discrete fracture and discrete vug network model. J Petrol Sci Eng 195:107626. https://doi.org/10.1016/j.petrol.2020.107626*10.1016/j.petrol.2020.107626

Wei W, Jiang Q, Ye Z, Xiong F, Qin H (2021) Equivalent fracture network model for steady seepage problems with free surfaces. J Hydrol 603:127156. https://doi.org/10.1016/j.jhydrol.2021.127156*10.1016/j.jhydrol.2021.127156

Weijermars R, Khanal A (2019) High-resolution streamline models of flow in fractured porous media using discrete fractures: implications for upscaling of permeability anisotropy. Earth-Sci Rev 194:399–448. https://doi.org/10.1016/j.earscirev.2019.03.011*10.1016/j.earscirev.2019.03.011

Xing K, Qian J, Ma H, Luo Q, Ma L (2021a) Characterizing the relationship between non-Darcy effect and hydraulic aperture in rough single fractures. Water Resour Res 57. https://doi.org/10.1029/2021WR030451*10.1029/2021WR030451

Xing K, Qian J, Zhao W, Ma H, Ma L (2021b) Experimental and numerical study for the inertial dependence of non-Darcy coefficient in rough single fractures. J Hydrol 603:127148. https://doi.org/10.1016/j.jhydrol.2021.127148*10.1016/j.jhydrol.2021.127148

Xue P, Wen Z, Park E, Jakada H, Zhao D, Liang X (2022) Geostatistical analysis and hydrofacies simulation for estimating the spatial variability of hydraulic conductivity in the Jianghan Plain, central China. Hydrogeol J 30:1135–1155. https://doi.org/10.1007/s10040-022-02495-4*10.1007/s10040-022-02495-4

Yaghoubi A (2019) Hydraulic fracturing modeling using a discrete fracture network in the Barnett Shale. Int J Rock Mech Min 119:98–108. https://doi.org/10.1016/j.ijrmms.2019.01.015*10.1016/j.ijrmms.2019.01.015

Younes A, Koohbor B, Fahs M, Hoteit H (2023) An efficient discontinuous Galerkin - mixed finite element model for variable density flow in fractured porous media. J Comput Phys 477:111937. https://doi.org/10.1016/j.jcp.2023.111937*10.1016/j.jcp.2023.111937

Young NL, Simpkins WW, Reber JE, Helmke MF (2020) Estimation of the representative elementary volume of a fractured till: a field and groundwater modeling approach. Hydrogeol J 28:781–793. https://doi.org/10.1007/s10040-019-02076-y*10.1007/s10040-019-02076-y

Zareidarmiyan A, Parisio F, Makhnenko RY, Salarirad H, Vilarrasa V (2021) How equivalent are equivalent porous media? Geophys Res Lett 48 https://doi.org/10.1029/2020GL089163*10.1029/2020GL089163

Zeng Y, Sun F, Zhai H (2021) Numerical study on application conditions of equivalent continuum method for modeling heat transfer in fractured geothermal reservoirs. Processes 9:1020. https://doi.org/10.3390/pr9061020*10.3390/pr9061020

Zhang L, Xia L, Yu Q (2017) Determining the REV for fracture rock mass based on seepage theory. Geofluids 2017:1–8. https://doi.org/10.1155/2017/4129240*10.1155/2017/4129240

Zhang Q, Liu Q, He G (2020) Reexamining the necessity of adding water curtain borehole with improved understanding of water sealing criterion. Rock Mech Rock Eng 53:4623–4638. https://doi.org/10.1007/s00603-020-02194-0*10.1007/s00603-020-02194-0

Zhang X, Ma F, Dai Z, Wang J, Chen L, Ling H, Soltanian MR (2022) Radionuclide transport in multi-scale fractured rocks: a review. J Hazard Mater 424:127550. https://doi.org/10.1016/j.jhazmat.2021.127550*10.1016/j.jhazmat.2021.127550

Zhao L, Jiang H, Zhang S, Yang H, Sun F, Qiao Y, Zhao L, Chen W, Li J (2018) Modeling vertical well in field-scale discrete fracture-matrix model using a practical pseudo inner-boundary model. J Petrol Sci Eng 166:510–530. https://doi.org/10.1016/j.petrol.2018.02.061*10.1016/j.petrol.2018.02.061

Zhao Y, Jiang H, Rahman S, Yuan Y, Zhao L, Li J, Ge J, Li J (2019) Three-dimensional representation of discrete fracture matrix model for fractured reservoirs. J Petrol Sci Eng 180:886–900. https://doi.org/10.1016/j.petrol.2019.06.015*10.1016/j.petrol.2019.06.015

Zheng X, Yang Z, Wang S, Chen Y, Hu R, Zhao X, Wu X, Yang X (2021) Evaluation of hydrogeological impact of tunnel engineering in a karst aquifer by coupled discrete-continuum numerical simulations. J Hydrol 597:125765. https://doi.org/10.1016/j.jhydrol.2020.125765*10.1016/j.jhydrol.2020.125765